

# A New 3-D Picture of the Milky Way with Classical Cepheids

Dorota M. Skowron,<sup>1\*</sup> Jan Skowron,<sup>1</sup> Przemek Mróz,<sup>1</sup> Andrzej Udalski,<sup>1</sup>  
Paweł Pietrukowicz,<sup>1</sup> Igor Soszyński,<sup>1</sup> Michał K. Szymański,<sup>1</sup>  
Radosław Poleski,<sup>2,1</sup> Szymon Kozłowski,<sup>1</sup> Krzysztof Ulaczyk,<sup>3,1</sup>  
Krzysztof Rybicki,<sup>1</sup> Patryk Iwanek,<sup>1</sup>

<sup>1</sup>Warsaw University Observatory, Aleje Ujazdowskie 4, 00-478 Warsaw, Poland,

<sup>2</sup>Department of Astronomy, Ohio State University,  
140 W. 18th Ave., Columbus, OH 43210, USA

<sup>3</sup>Department of Physics, University of Warwick, Coventry CV4 7AL, UK

\*E-mail: dszczyg@astrouw.edu.pl

**The global view of the Milky Way as a barred spiral galaxy was inferred from various tracers, *e.g.*, star counts or radio maps of Galactic gas, as well as from our extrapolation of structures seen in other galaxies. However, distances to these tracers are measured indirectly and are model-dependent, so the exact structure of our Galaxy is still under debate. We present a new comprehensive picture of our Galaxy in three-dimensions based on the positions in the sky and precisely measured distances of thousands of newly detected Classical Cepheids. We unravel, for the first time, the real structure of our Galaxy as seen via the young stellar population. This new picture allows us to precisely constrain the Galactic disk shape and dig into the recent history of our Galaxy.**

Classical Cepheids are young ( $< 300$  million years old) supergiants with luminosities in

the range of  $100 - 10,000L_{\odot}$ , pulsating with periods 1-100 days. This makes them visible at extragalactic distances and, in our Galaxy, detectable even through clouds of gas and dust obscuring less luminous stars. Cepheids obey the pulsation period-luminosity (P-L) relation (1), which allows determining the absolute magnitude of the Cepheid from its period and thus – by comparison with the apparent magnitude – its distance, provided the interstellar extinction is known. While the large and often non-standard extinction may pose a problem in the optical wavelengths, switching to the infrared (IR) bands minimizes these uncertainties. The detection of Cepheids in the optical bands is relatively easy owing to their characteristic saw-tooth light curves and relatively large amplitudes, contrary to the IR bands, where the shape becomes more sinusoidal and hard to distinguish from variables of other types. Similarly, Cepheids can be mimicked by other variable stars in the optical bands if the number of measurements is limited (below 80-100 epochs) and the survey time span is short ( $< 1 - 2$  years) (2).

The majority of 2325 Galactic Cepheids analyzed here are the newest discoveries by the large-scale survey of the Galactic disk and Center conducted during the fourth phase of the Optical Gravitational Lensing Experiment (OGLE-IV) project (3). This is a long-term survey focused on discovery and detailed classification of variable stars. The 1296 Classical Cepheids recently detected by the survey (2), together with 104 objects discovered by OGLE in the past years, more than doubled the number of known Galactic variables of this type. The magnitude range of the dedicated survey of the Galactic plane – 11–18 mag in the *I*-band – enables identification of Cepheids as distant as the expected boundary of the Galactic disk, which has been impossible until now. The OGLE survey covered practically the entire range of the Galactic disk available from its site at Las Campanas, Chile (see Fig 1).

Cepheids closer than 4 kpc are too bright and saturated in the OGLE survey images. Therefore, the OGLE sample has been complemented with brighter objects from the list of Galactic Cepheids (4), coming mostly from the General Catalog of Variable Stars (GCVS) (5) and the

ASAS (6) survey. We also supplement the list with ATLAS (7) Cepheids that we identified in their recent catalog. For details on the Cepheid sample used in this study please refer to the Supplementary Materials (8).

The Galactic dust resides predominantly in the vicinity of the Galactic plane, where Cepheids live, and is the source of the large extinction in the optical bands. To minimize this problem, the distances to individual objects from the final sample were calculated based on the mid-IR photometry obtained by the Spitzer and WISE satellites, with the use of the most recent P-L relations (9), and a constant extinction value. For all of them the Cartesian coordinates with the origin in the Sun were derived for studying their 3-D distribution (8).

Fig. 1 presents the OGLE map of the Galaxy for the young stellar population – the view projected on the sky (Fig. 1a) and the face-on view (Fig. 1b), where the individual Cepheids are marked with green dots on top of the four-arm spiral galaxy model consistent with neutral hydrogen (HI) measurements in our Galaxy (10). We clearly see areas of higher Cepheid density indicating the non-uniform Galactic structure or the regions of increased star formation. The side view (Fig. 1a) shows, that the young stellar disk of the Milky Way (as traced by the Cepheids) is warped and has a varying width. The warping of the disk has been observed before, both in HI (11) and in various young environments (12–14), as well as kinematically (15, 16), although its full extent and shape have not yet been fully constrained. Here we have an opportunity to characterize the warp in detail based on a large sample of standard candles covering the majority of the Galactic disk.

We subdivide the Galaxy into 12 slices (of unequal azimuthal width) of the Galactocentric polar coordinate system with  $\phi = 0$  deg pointing to the Sun (Fig. 2a). The disk is clearly not flat – the warp is strikingly noticeable in many directions that are sufficiently well populated with Cepheids. The warping of the disk begins at the distance of about 8 kpc and becomes steeper at  $\sim 10$  kpc, reaching out to the very edge of the Galaxy. The disk warps toward negative Z

within  $0^\circ < \phi < 135^\circ$  and toward positive Z at  $165^\circ < \phi < 330^\circ$ , although the exact boundary is difficult to assess, due to lower number of known Cepheids on the other side of the Galactic Center.

We model the young disk by fitting the distribution of Cepheids with a simple exponential formula (8). We measure the disk scale height  $H = 80.8 \pm 2.8$  pc and the distance of the Sun from the Galactic plane  $z_0 = 24.6 \pm 2.8$  pc (see Fig. 5). To further illustrate the warping of the disk and guide the eye, we fit a simple model surface to the Cepheid distribution, which is shown in Fig. 2b from three selected viewing angles.

Classical Cepheids are excellent tracers of stellar age. Their pulsation period is monotonically correlated with age (17), making it possible to perform an age tomography of the Milky Way. The majority of Cepheids in our sample formed between 30 to 130 million years ago (Fig. 3a). The spatial distribution of ages (Fig. 3b) clearly shows that the closer to the Galactic Center, the younger objects we observe, and that the most recent star formation episodes must have occurred in the regions closer to the Galactic Center than the Sun. Accordingly, regions toward the anticenter contain the older Cepheids from our sample, although the oldest Cepheids with ages well exceeding 100 Myr, can be found all over the Milky Way. This is further pictured in Figs 3c-e, where the distribution of Cepheids in three non-overlapping age bins is shown.

There are several distinct features in the spatial distribution of Cepheids (Fig. 3f). Since these features are located mainly in the area monitored by OGLE – where the Cepheid detection efficiency is very high – they are most likely real, rather than the result of a detection bias. The most prominent overdensity is formed by stars from a narrow age range (around 68 Myr) – see Fig. 3d. The traces of this arc-shaped overdensity were previously associated with the spiral arm (18), however, our sample shows that it is located in between the Sun and the nearest, so called, Sagittarius Arm, rather than within this arm. Moreover, our large sample shows, for the first time, that this Cepheid overdensity does not follow a consistent pitch angle of the spiral

arms in the Galaxy (19).

There are other distinct overdensities noticeable in the general picture of the Galactic Cepheids (Fig. 3f). In Fig. 3g we identify three main overdensities as O1, O2 and O3. While less pronounced in space than the previously mentioned feature O2, the ages of Cepheids within the two remaining overdensities are also coherent and the fact that they lie close to each other and have similar ages (compare panels c and e), strongly suggests their common origin in the past star formation episodes in certain parts of the Galaxy.

We perform a simple simulation, in which we select stars from three age bins characteristic for the overdensities marked in Fig. 3g (see (8) for details on the selection criteria). Median age values in these three groups are 35, 68 and 91 Myr. Then we ask whether there could have been a star formation episode in one of the spiral arms of the Milky Way in the past, that after a given time (after the Galaxy has rotated), would produce the current observed distribution of Cepheids. The results of this exercise are presented in Fig. 4, where each row focuses on one of the overdensities: O1 (panels a-c), O2 (panels d-f), and O3 (panels g-i). In each row, the first image shows the current observed distribution of Cepheids, where the selected overdensity is highlighted. The middle panel presents the view of the spiral arms of the Galaxy, as it looked 35 (b), 68 (e) and 91 (h) million years ago (following an assumed rotational period of the spiral pattern equal to 260 Myr (19)). On top of that, we inject a star formation episode that is happening in a region(s) along the spiral arms at that time. Finally, the last panels (c, f, i) show how those star formation regions would look now (after 35, 68 and 91 Myr respectively), taking into account the typical velocity of disk stars (20) and 15 km/s velocity dispersion.

Given these simple assumptions, we see a surprisingly good correlation between the real and artificially created distributions of Cepheids – both in the shape of the overdensity, as well as in its internal dispersion. Cepheids that were born in a spiral arm, do not currently follow the exact location of that arm, which can be explained by the different rotation velocity of the

density waves and the stars. This is most pronounced in the case of the oldest group O3 (Fig. 4g-i), where the overdensity falls directly in between the arms of Perseus and Norma-Cygnus, near which it was most likely born. Interestingly, our model also reveals that the Sun was located near the actively star forming spiral arm (Fig. 4e) in the era of the Cretaceous–Tertiary mass extinction that occurred approximately 66 Myr ago and led to the sudden extinction of about three quarters of the Earth’s species (21).

In summary, the OGLE 3-D picture of the Milky Way is the first one based on a large number of individual objects with very precisely determined distances. It represents the young stellar population that extends to over 20 kpc covering a significant part of our Galaxy, thus making it possible, for the first time, to assess the extent and shape of the young stellar disk. While the detailed modelling of the Milky Way structure is beyond the scope of this paper, we show that a very simple model can reproduce the current picture of the young stellar disk of the Milky Way, where classical Cepheids form structures that do not necessarily trace the spiral arms, but their location is shifted with respect to the aforementioned. The picture of the Milky Way presented in this paper can be better constrained by more complex modeling of the Cepheid sample, which is beyond the scope of this paper. In the future, it should be complemented with faint Cepheids detected by OGLE-like deep sky surveys of the northern hemisphere – the regions unavailable to the OGLE survey.

## References

1. H. S. Leavitt, E. C. Pickering, *Harvard College Observatory Circular* **173**, 1 (1912).
2. A. Udalski **152**, 01002 (2017).
3. A. Udalski, M. K. Szymański, G. Szymański, *Acta Astron.* **65**, 1 (2015).
4. P. Pietrukowicz, *et al.*, *Acta Astron.* **63**, 379 (2013).

5. N. N. Samus', E. V. Kazarovets, O. V. Durlevich, N. N. Kireeva, E. N. Pastukhova, *Astronomy Reports* **61**, 80 (2017).
6. G. Pojmanski, *Acta Astron.* **52**, 397 (2002).
7. A. N. Heinze, *et al.*, *ArXiv e-prints* (2018).
8. Materials and methods are available as supplementary materials at the Science website.
9. S. Wang, X. Chen, R. de Grijs, L. Deng, *Astrophys. J.* **852**, 78 (2018).
10. E. S. Levine, L. Blitz, C. Heiles, *Science* **312**, 1773 (2006).
11. F. J. Kerr, G. Westerhout p. 167 (1965).
12. M. Miyamoto, Z. Zhu, *Astron. J.* **115**, 1483 (1998).
13. I. Yusifov, I. Küçük, *Astron. Astrophys.* **422**, 545 (2004).
14. M. W. Feast, J. W. Menzies, N. Matsunaga, P. A. Whitelock, *Nature* **509**, 342 (2014).
15. R. L. Smart, R. Drimmel, M. G. Lattanzi, J. J. Binney, *Nature* **392**, 471 (1998).
16. E. Poggio, *et al.*, *ArXiv e-prints* (2018).
17. G. Bono, *et al.*, *Astrophys. J.* **621**, 966 (2005).
18. A. K. Dambis, *et al.*, *Astronomy Letters* **41**, 489 (2015).
19. J. P. Vallée, *The Astronomical Review* **13**, 113 (2017).
20. Gaia Collaboration, *et al.*, *ArXiv e-prints* (2018).
21. P. R. Renne, *et al.*, *Science* **339**, 684 (2013).

22. I. Soszyński, *et al.*, *Acta Astron.* **67**, 297 (2017).
23. I. Soszyński, *et al.*, *Acta Astron.* **61**, 285 (2011).
24. R. A. Benjamin, *et al.*, *Publ. Astron. Soc. Pac.* **115**, 953 (2003).
25. E. Churchwell, *et al.*, *Publ. Astron. Soc. Pac.* **121**, 213 (2009).
26. E. L. Wright, *et al.*, *Astron. J.* **140**, 1868 (2010).
27. A. Mainzer, *et al.*, *Astrophys. J.* **731**, 53 (2011).
28. P. Klagyivik, L. Szabados, *Astron. Astrophys.* **504**, 959 (2009).
29. P. Pietrukowicz, *et al.*, *Astrophys. J.* **811**, 113 (2015).
30. S. Gillessen, *et al.*, *Astrophys. J.* **837**, 30 (2017).
31. D. Foreman-Mackey, D. W. Hogg, D. Lang, J. Goodman, *Publ. Astron. Soc. Pac.* **125**, 306 (2013).
32. B.-C. Koo, *et al.*, *Publ. Astron. Soc. Pac.* **129**, 094102 (2017).

## Acknowledgments

This publication makes use of data products from the Wide-field Infrared Survey Explorer, which is a joint project of the University of California, Los Angeles, and the Jet Propulsion Laboratory/California Institute of Technology, funded by the National Aeronautics and Space Administration. This work is based in part on observations made with the Spitzer Space Telescope, which is operated by the Jet Propulsion Laboratory, California Institute of Technology under a contract with NASA. The OGLE project has received funding from the National Science Center (NCN), Poland through grant MAESTRO 2014/14/A/ST9/00121 to A.U. D.M.S. is



partially supported by the NCN under the grant no. 2013/11/D/ST9/03445. I.S. acknowledges support from the NCN, grant MAESTRO 2016/22/A/ST9/00009. P.M. acknowledges support from the Foundation for Polish Science – Program START.

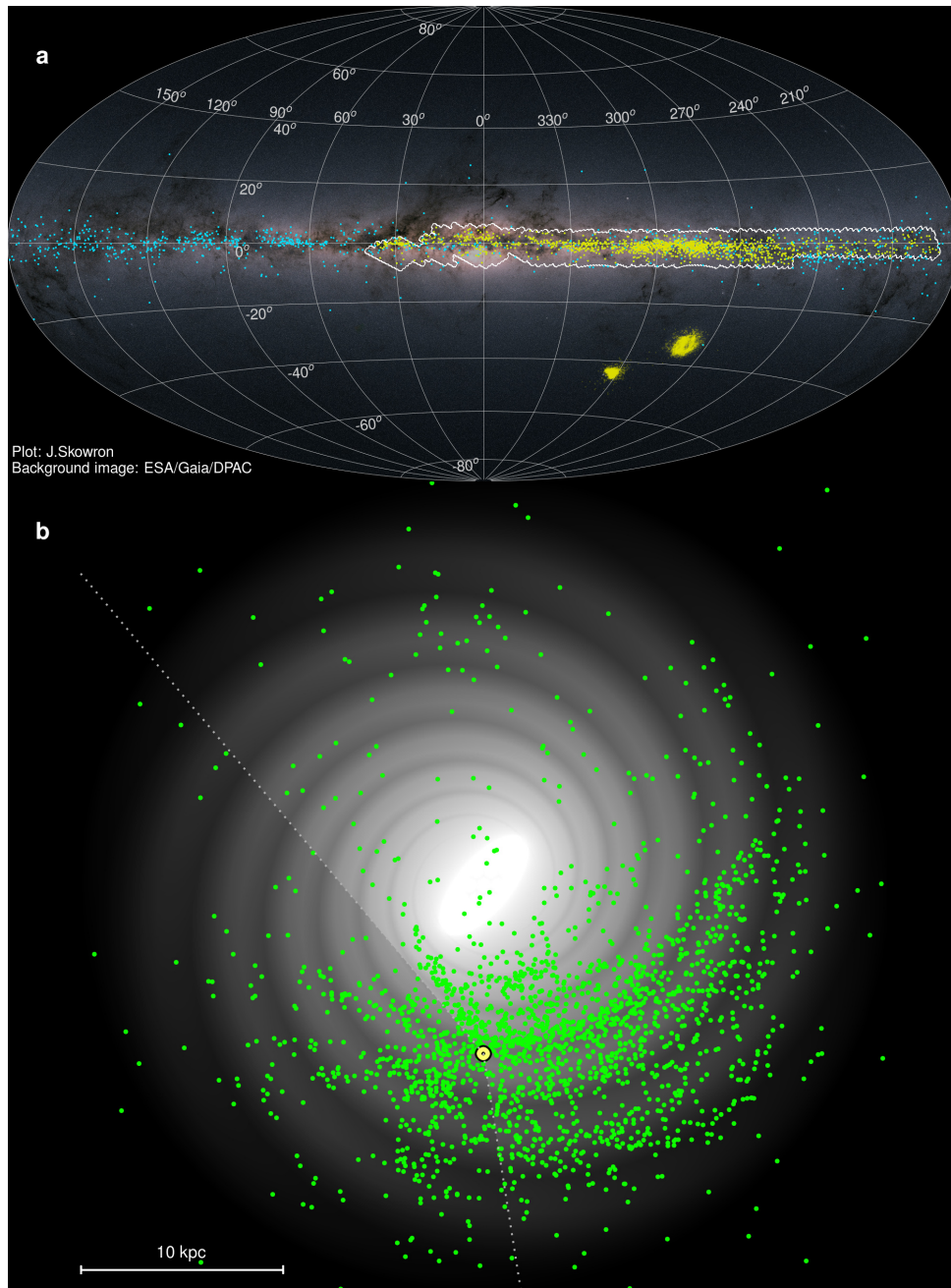
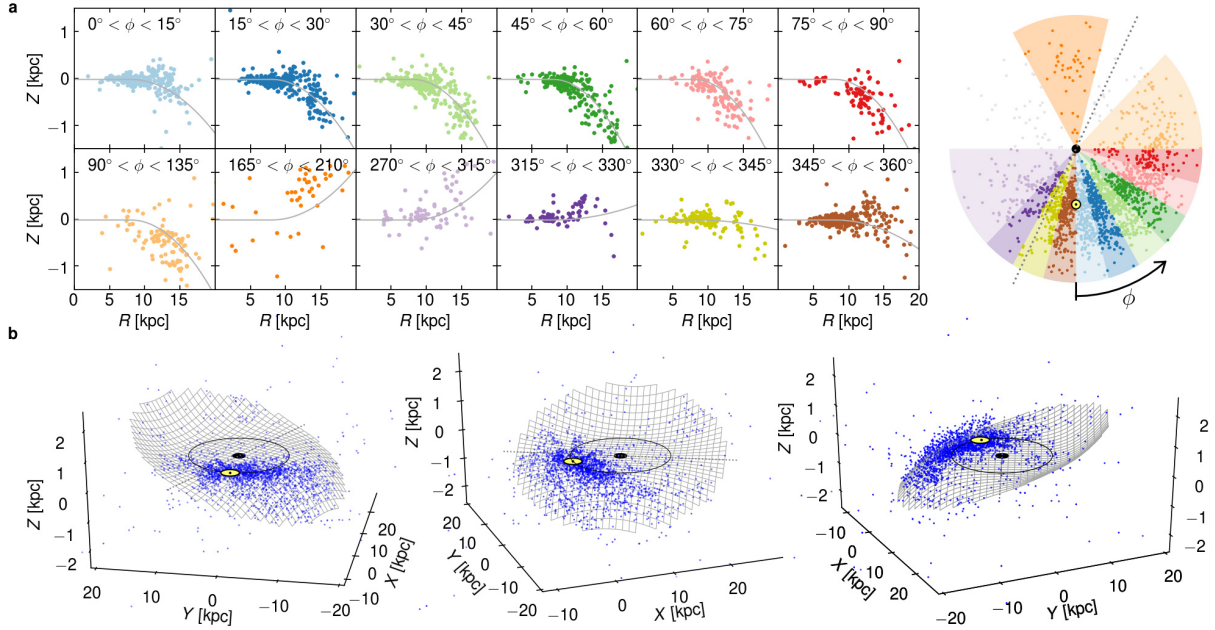


Figure 1: **The distribution of Galactic Classical Cepheids.** (a) The on-sky view of the Milky Way in Galactic coordinates, with all known Classical Cepheids in the Milky Way and in the Magellanic Clouds. Cepheids from the OGLE collection of variable stars are shown with yellow dots, while all other discoveries with cyan dots. The white contours mark the OGLE coverage of the Galactic plane ( $-170 < l < +40$  deg,  $-6 < b < +3$  deg). The background image is the photograph of the Milky Way based on Gaia satellite measurements (Copyright: ESA/Gaia/DPAC). (b) The top view of our Galaxy with all 2325 Cepheids used in this study marked with green dots. The background image represents a four-arm spiral galaxy model consistent with neutral hydrogen measurements in our Galaxy (here the spiral structure is illustrated by the logarithmic spirals). The Sun is marked with a yellow disk, while the dashed lines show the angular extent of the OGLE fields ( $-170 < l < +40$  deg).



**Figure 2: The Milky Way warp.** (a) The warping of the disk of our Galaxy is presented by slicing up the disk into 12 slices in the Galactocentric polar coordinate system with  $\phi = 0$  deg pointing to the Sun. Each slice is shown with a different color, as indicated in the pie chart on the right, and the same colors are used to show the distribution of Cepheids along the Galactic distance  $R$  versus distance from the Galactic plane  $Z$  in those twelve panels (left). The Sun is marked with the yellow disk, while the Galactic Center with a black disk. Gray lines are the cross-cuts of the model surface (panel b) within a given slice. The dotted line on the pie chart separates parts of the Galaxy warped toward negative and positive  $Z$ . (b) An illustration of the Milky Way warp from three selected viewing angles. The Cepheids are marked with blue dots, and the gray grid is a model surface fit to the Cepheid distribution (8).

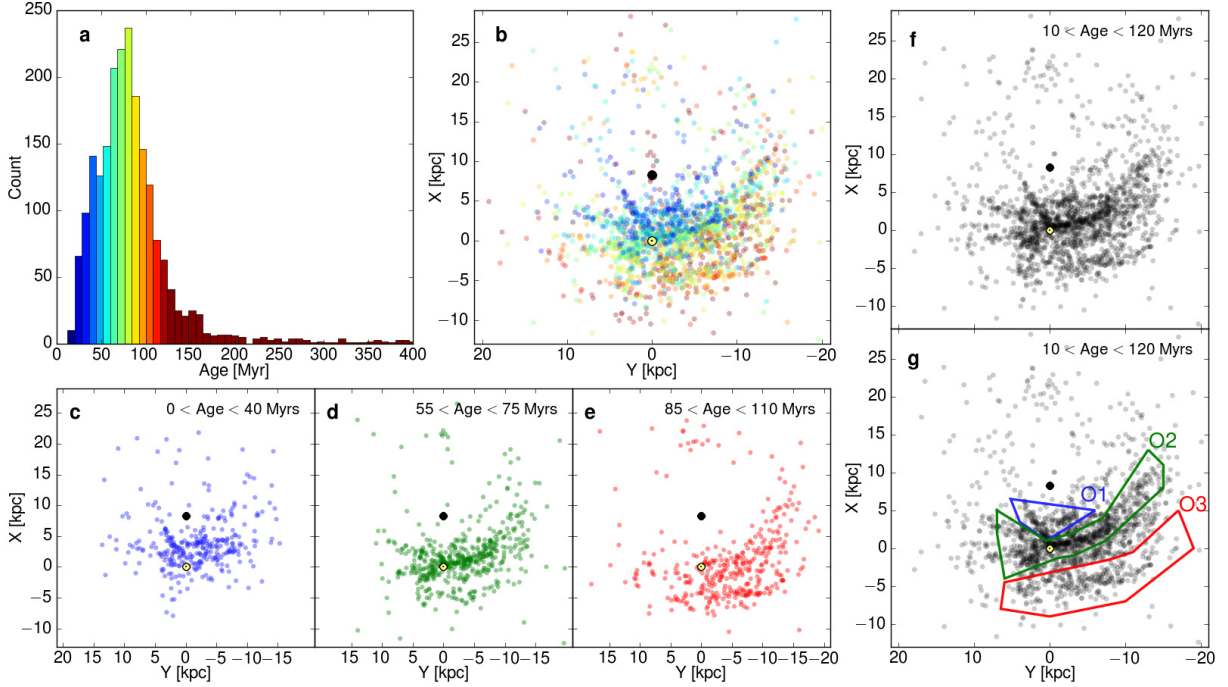


Figure 3: **Ages of Galactic Classical Cepheids.** (a) The age histogram of Galactic Classical Cepheids in our sample. (b) The face-on view, showing the Cepheid distribution in the Galaxy, with colors corresponding to Cepheid ages as indicated in panel (a). The Sun is marked with a yellow disk, while the Galactic Center with the black disk. (c-e) The age tomography of the Milky Way in three selected age bins, as indicated in the top part of each panel. Each age bin reveals Cepheid overdensities. (f) Cepheids in a wide age range  $10 < \text{Age} < 120$  Myr, but without color coding, to emphasize the most prominent overdensities in the Cepheid distribution. (g) Same as panel (f), but showing the selection regions for three main overdensities O1, O2, O3, that are further studied in more detail in Fig. 4.

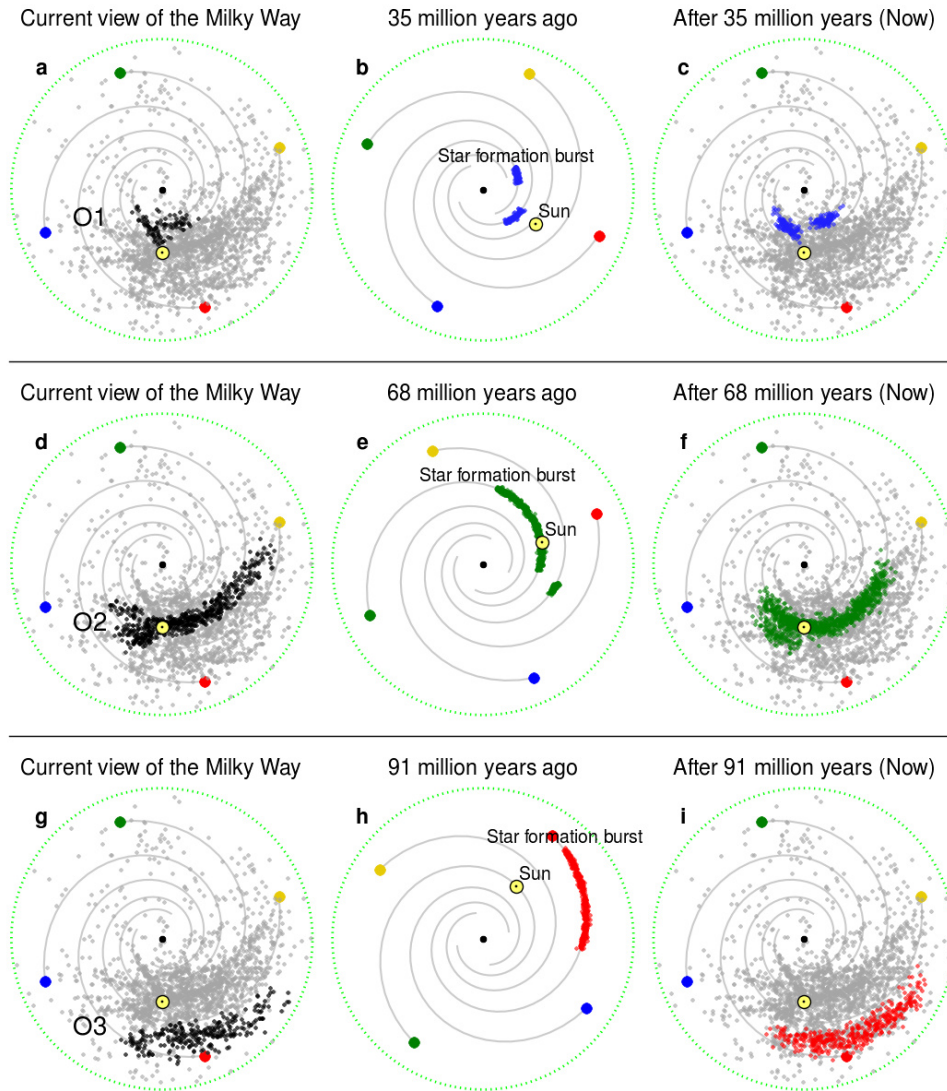


Figure 4: **The possible origin of the Cepheid structures.** (a) The face-on view of our Galaxy, where all Cepheids are marked with gray dots, and the Cepheids that belong to overdensity O1 (median age 35 Myr) are shown with black dots. The Sun is marked with a yellow disk, while the Galactic Center with the black disk. The locations of the spiral arms are highlighted with colored dots – Perseus arm (yellow), Sagittarius-Carina arm (green), Scutum-Crux-Centaurus (blue) and Norma-Cygnus (red). (b) The location of the Galaxy’s spiral arms 35 Myr ago, with an artificial star formation region along the Scutum-Crux-Centaurus and Norma-Cygnus arms marked in blue. (c) The current location of the artificial star formation region (blue) on top of the distribution of all Cepheids from our sample (gray). (d-f) Same as panels (a-c), but for the overdensity O2 with a median age of 68 Myr. (g-i) Same as panels (a-c), but for the overdensity O3 with a median age of 91 Myr.

# Supplementary Materials

## Materials and methods

### The Cepheid sample

The sample of Classical Cepheids used in this work consists of 2325 objects. The majority were found by the OGLE survey: 1296 objects from the OGLE-IV Collection of Galactic Cepheids (2), 68 objects from the OGLE-IV collection of Galactic bulge Cepheids (22), and 36 objects from the OGLE-III catalog of variable stars in the Galactic bulge (23) and disk (4). The total number of Classical Cepheids from the OGLE survey is 1400. The remaining 925 stars are from various sources: 603 from the General Catalog of Variable Stars (GCVS), 61 from the ASAS catalogs (6), and 15 from over a dozen other sources.

We also used the recent Asteroid Terrestrial-impact Last Alert System (ATLAS) catalog of variable stars (7) to identify Classical Cepheids. Following the suggestions of the authors, we selected all stars with the 'PULSE' classification that have a long-period fit or a short-period fit leading to a master period longer than 1 day. We also selected stars that were not classified as 'PULSE' but have significant variations, and their master period is longer than 1 day. See the authors prescriptions for further details. The search resulted in almost 3000 Cepheid candidates with available light curves. Our analysis of the ATLAS time series was similar to the procedures applied to the OGLE photometry. We determined periods, amplitudes, and Fourier coefficients for all available light curves in both pass bands (cyan and orange) used by the ATLAS survey. Then, we selected and classified pulsating stars based on the visual inspection of their folded light curves, taking into account their position in the period–Fourier coefficients diagrams and ratios of the light amplitudes in the two ATLAS filters. The classification procedure returned 439 Classical Cepheids, 246 of which are new discoveries. We also identified 142 type II Cepheids and 61 anomalous Cepheids in the Cepheid candidate sample. The majority of the

remaining 2130 ATLAS objects turned out to be eclipsing binaries and spotted variables, and even some RR Lyrae type stars that were assigned a 1-day alias period.

The full list of 2325 genuine Classical Cepheids used in this work is presented in Table 1, including a reference to a discovery paper, whenever available. Otherwise we provide the source (*e.g.*, GCVS) or a database, in which the Cepheid was identified (*e.g.*, ATLAS).

### **MID-IR Data.**

The mid-IR observations of Cepheids are available from the Spitzer Space Telescope and the Wide-field Infrared Survey Explorer (WISE).

We utilized data from the “Galactic Legacy Infrared Mid plane Survey Extraordinaire” (GLIMPSE) Legacy Program of Spitzer and its extensions: GLIMPSE II, GLIMPSE 3D, GLIMPSE 360, Deep GLIMPSE and Vela-Carina, as well as from the “Spitzer Mapping of the Outer Galaxy” (SMOG) and “A Spitzer Legacy Survey of the Cygnus-X Complex” (Cygnus-X) Legacy Programs (24, 25), which we will collectively call the GLIMPSE data. The Spitzer observations of the Galactic plane were made in four IRAC (Infrared Array Camera) bands: I1=[3.6], I2=[4.5], I3=[5.8] and I4=[8.0] microns. For each Cepheid from our final list we extracted all available GLIMPSE observations within 1 arcsec search radius. We found matches for 1213 out of 2325 objects. The majority of Cepheids (938) had only one match in the GLIMPSE catalogs, while 275 were found in more than one GLIMPSE programs: 242 stars had 2 matches, 31 stars had 3 matches and 2 stars had 4 matches. We calculated weighted mean magnitudes for 1090, 1122, 756 and 715 Cepheids in I1, I2, I3 and I4 bands, respectively.

We also use the WISE data from the AllWISE Multiepoch Photometry Database, which provides all-sky time-series photometry from both the WISE cryogenic and NEOWISE post-cryogenic phases of the survey (26, 27). The observations were made in four bands: W1=[3.4], W2=[4.6], W3=[11.6], and W4=[22.1] microns. We found counterparts for 1958 out of 2325

Cepheids within 1 arcsec search radius. The number of points per light curve in the W1 band varied from 16 to over 500 with a median value of 60 points. We calculated weighted mean magnitudes for 1392, 1730, 1599 and 698 Cepheids in W1, W2, W3 and W4 bands, respectively.

### **Distances and extinction.**

The distance  $d$  in a given band  $\lambda$  can be calculated as:

$$d_{\lambda} = 10^{0.2(m_{\lambda} - M_{\lambda} - A_{\lambda}) + 1} \text{ pc}$$

where  $m_{\lambda}$  and  $M_{\lambda}$  are, respectively, the observed and absolute magnitudes of the star and  $A_{\lambda}$  is the extinction value. The absolute magnitudes can be calculated from the P-L relations. Here we use the most recent mid-IR P-L relations, derived for the Spitzer and WISE passbands (9) based on a sample of 288 Galactic Classical Cepheids. The extinction values in the Galaxy are high in the optical bands and depend on the exact direction, but become low and fairly independent of the line-of-sight in the mid-IR. We use the average value of the mid-IR extinction of 0.09 mag for all mid-IR bands (9). The error in distance introduced by accepting a constant extinction value should be very low for the vast majority of Cepheids (*e.g.*, the complete omission of extinction in the mid-IR results in barely  $\sim 4\%$  distance error).

In the first step, we estimate the distance to each object separately in all available Spitzer and WISE bands. Then the final distance value is calculated as a weighted average (with outlier rejection) of single-band distances. The weight in each band consist of two factors: the magnitude uncertainty in that band as reported by the survey, and the expected rms scatter of the Cepheid light curve in the given band, caused by its pulsational amplitude. Since the mid-IR amplitudes for the majority of Cepheids are not known, due to the low number of observations, we use their optical counterparts to estimate the mid-IR brightness changes. Most Cepheids in our sample have well covered *I*-band light curves, so their amplitude and thus the expected rms



scatter can be estimated. In the case when only the *V*-band light curve is available, we scale its *V*-band amplitude by a factor of 0.6 to obtain the *I*-band amplitude and rms scatter (28).

We then choose a subset of Cepheids with well covered light curves in all WISE bands. From those, we pick the ones with low photometric noise and estimate their mid-IR rms scatter. We found that for the majority of stars the rms scatter in the *I*-band is proportional to the rms scatter in all mid-IR bands with the proportionality constant close to 2. Therefore, we take the measured rms *I*-band scatter, divide it by 2, and use it as an uncertainty of the mean brightness as measured from a single mid-IR epoch, both for the Spitzer and WISE bands. The brightness uncertainty propagates to the distance uncertainty as  $\sigma_d = d \times \log(10) \times 0.2\sigma_{mag}$ . The final distance error is estimated as a geometric mean of the uncertainties of the single band distance measurements, used to calculate the Cepheid distance.

When averaging the distances, we found that the significant portion of rejected outlier measurements comes from the W3 and W4 bands, yielding systematically lower final distance values. We have not investigated this here in detail, however, we presume that this may originate from blending effects within a large PSF of the WISE satellite – the P-L relations (9) were determined using a sample of Cepheids in less crowded regions, and may not be applicable to all our Cepheids. To avoid underestimating distances, W3 and W4 distance measurements are rejected whenever two or more distance measurements from shorter wavelengths (either Spitzer or WISE) are available for a given star. However, this cannot be applied to bright, closeby stars, which are saturated in shorter mid-IR bands, and so their distances are usually determined solely from the W3 and W4 bands.

Table 1 provides mean magnitudes and their uncertainties in all eight mid-IR bands, as well as the final distance value and its uncertainty for all Cepheids in our sample.

### **Cartesian coordinates.**

The 3-D distribution of Cepheids in our sample is studied in the Cartesian coordinate system with the origin in the Sun:

$$X = d \times \cos l \cos b$$

$$Y = d \times \sin l \cos b$$

$$Z = d \times \sin b$$

where  $l$  and  $b$  are the Galactic coordinates of the star and  $d$  is its distance from the Sun. We adopt the distance between the Galactic Center and the Sun of 8.3 kpc (29, 30).

### **Disk scale height.**

We model the vertical distribution of Cepheids using a simple exponential model of the thin disk, which has two free parameters: the scale height  $H$  and the distance of the Sun from the Galactic plane  $z_0$ . The density of stars varies as:

$$n(z) = \frac{1}{2H} \exp\left(-\frac{|z|}{H}\right),$$

where  $z = z_0 + d \sin b$ ,  $d$  is the distance to the Cepheid and  $b$  is its Galactic latitude. The best-fit model is found by maximizing the likelihood function, defined as  $\ln \mathcal{L} = \sum_i \ln n(z_i)$ . The summation is performed over all stars within 10 kpc of the Galactic Center (to minimize the effect of the disk's warp) and Galactic latitudes  $|b| \leq 4^\circ$ . The best-fit parameters are  $H = 80.8 \pm 2.8$  pc and  $z_0 = 24.6 \pm 2.8$  pc. This is in general agreement with past determinations. The histogram of  $z$  together with the fit model is presented in Fig. 5, while different fit parameters are listed in Table 2. The uncertainties are estimated using the Markov chain Monte Carlo technique (31) and represent 68% confidence range of marginalized posterior distributions. We assume uniform priors on  $H$  and  $z_0$  over the ranges 0 to 1 kpc and  $-1$  to 1 kpc, respectively.

If Cepheids located farther than 10 kpc from the Galactic Center are included in the model, the best-fit  $z_0$  increases, which is the signature of the Galactic disk's warp.

To guide the eye, we also fit a polynomial surface to the distribution of Cepheids in the form:

$$\begin{aligned} Z(R, \phi) &= -z_0 && \text{for } R < R_0 \\ Z(R, \phi) &= -z_0 + z_1(R - R_0)^2 \cos(\phi - \phi_0) && \text{for } R \geq R_0 \end{aligned}$$

By minimizing the sum of squares of orthogonal distances from the data points to the surface  $\chi^2 = \sum_i \|\vec{R}_i - \vec{R}_{\text{model}}\|^2$ , we obtain the best-fit parameters:  $z_0 = 17.8$  pc (in good agreement with the Sun's height from the thin disk exponential model),  $z_1 = +0.0142 \text{ kpc}^{-1}$  and  $\phi_0 = 244^\circ$  for fixed  $R_0 = 8$  kpc.

### **Modeling the overdensities.**

In order to select groups of Cepheids for overdensity modeling, that are correlated in age and space, we first manually select regions with main prominent overdensities O1, O2 and O3 as marked in Fig. 3g. The median ages of stars falling into the marked regions are 43, 66, and 88 Myr, respectively, and standard deviations are 18-20 Myr. Since our age estimates are not exact, we expect that stars that formed together might show slightly different ages. To remove the contamination from other star formation episodes we remove from our sample all stars with ages deviating more than 40% from the median age of each of the three groups. This is an iterative process that converged to the following values: 35, 68 and 91 Myr. The samples are shown as black points in the left panels of Fig. 4.

Stars in the Galaxy follow a flat rotation curve starting from the radius of about 7-8 kpc, with the rotational velocity of about 230 km/s, and have smaller velocity values at shorter radii. We assume a simple rotation curve inspired by the recent measurements (20) in the Solar neigh-

borhood of 180, 190, 215, 225 and 230 km/s for Galactocentric radii of 4, 5, 6, 7 and 8 kpc, respectively.

In the next step, for each age group, we pick a region within one of the spiral arms, populate it randomly with stars and assign them the rotation velocities following the rotation curve mentioned above, with an additional of (20, 10) km/s dispersion in the  $(\phi, R)$  directions. The positions of these young Cepheid candidates are shown in the central panels of Fig. 4. The rotation of the Galaxy to the present day is shown in the right panels of this figure.

We use a simple four-arm spiral structure model with the pitch angle of 12.4 degrees (32). We mark all arms with colored dots for easier identification – Perseus arm (yellow), Sagittarius-Carina arm (green), Scutum-Crux-Centaurus (blue) and Norma-Cygnus (red).

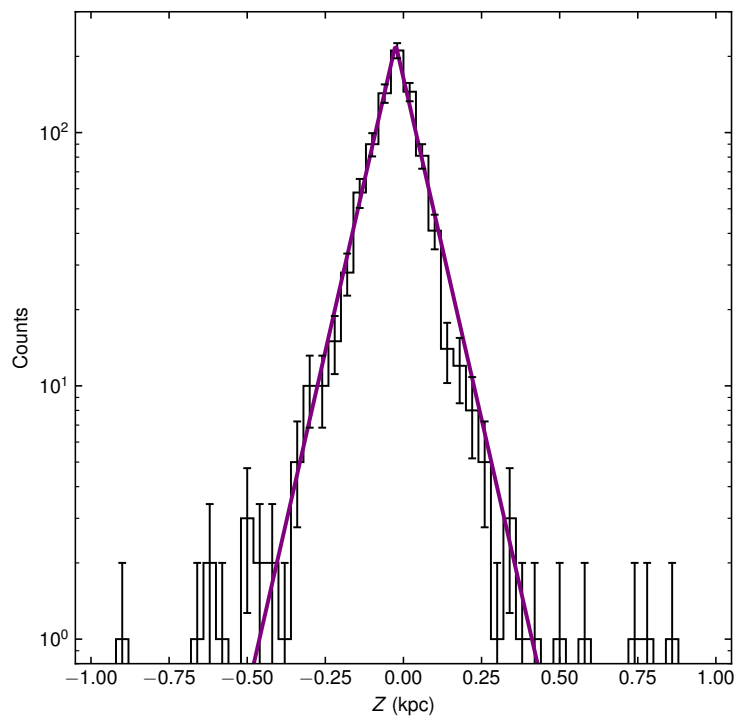


Figure 5: Histogram of distances of Cepheids from the Galactic plane. (Objects located within 10kpc of the Galactic Center and  $|b| \leq 4^\circ$ ). The purple line marks the best-fit exponential model.

Source	Cepheid ID	I1 (mag)	I2 (mag)	I3 (mag)	I4 (mag)	W1 (mag)	W2 (mag)	W3 (mag)	W4 (mag)	d (pc)	$\sigma_d$ (%)	Age (Myr)
OGLE-IV	GD1267.25.15316	10.141 ± 0.041	10.097 ± 0.042	10.109 ± 0.063	10.005 ± 0.035	9.956 ± 0.015	9.947 ± 0.013	0.000 ± 0.000	0.000 ± 0.000	6660	0.3	91
GCVS	V979...Mon	0.000 ± 0.000	0.000 ± 0.000	0.000 ± 0.000	0.000 ± 0.000	9.273 ± 0.020	9.249 ± 0.021	9.235 ± 0.035	0.000 ± 0.000	3136	0.5	142
GCVS	CE...Pup	0.000 ± 0.000	0.000 ± 0.000	0.000 ± 0.000	0.000 ± 0.000	0.000 ± 0.000	7.574 ± 0.051	7.532 ± 0.050	0.000 ± 0.000	12685	1.8	15
OGLE-IV	GD1326.28.29816	9.398 ± 0.062	9.423 ± 0.065	9.321 ± 0.063	9.308 ± 0.056	9.400 ± 0.033	9.403 ± 0.033	9.363 ± 0.035	0.000 ± 0.000	7969	0.6	58
GCVS	CC...Car	8.639 ± 0.056	8.559 ± 0.075	8.739 ± 0.080	0.000 ± 0.000	8.664 ± 0.050	8.646 ± 0.050	8.185 ± 0.051	6.190 ± 0.057	4568	0.8	72
OGLE-IV	GD1326.13.19638	10.197 ± 0.048	10.110 ± 0.045	10.267 ± 0.100	10.054 ± 0.061	10.278 ± 0.039	10.215 ± 0.039	10.133 ± 0.045	0.000 ± 0.000	10943	1.8	60
ATLAS	J098.2496+07.1745	9.422 ± 0.043	9.383 ± 0.039	0.000 ± 0.000	0.000 ± 0.000	9.481 ± 0.014	9.413 ± 0.016	9.425 ± 0.030	0.000 ± 0.000	5260	1.1	90
Tamoka2017	Lp20A	10.452 ± 0.088	10.179 ± 0.093	9.931 ± 0.092	10.080 ± 0.090	0.000 ± 0.000	0.000 ± 0.000	0.000 ± 0.000	0.000 ± 0.000	14646	3.7	41
OGLE-III	OGLE-GD-CEP-0003	0.000 ± 0.000	0.000 ± 0.000	0.000 ± 0.000	0.000 ± 0.000	11.058 ± 0.055	11.127 ± 0.055	0.000 ± 0.000	0.000 ± 0.000	13858	2.1	73
ATLAS	I103.5793-11.4393	0.000 ± 0.000	0.000 ± 0.000	0.000 ± 0.000	0.000 ± 0.000	8.895 ± 0.023	8.864 ± 0.023	8.797 ± 0.035	0.000 ± 0.000	6181	0.5	59
GCVS	V1364.Cyg	7.928 ± 0.077	7.904 ± 0.073	0.000 ± 0.000	0.000 ± 0.000	0.000 ± 0.000	7.774 ± 0.051	7.647 ± 0.050	6.805 ± 0.106	6036	1.6	37
ASAS	J052610+1151.3	0.000 ± 0.000	0.000 ± 0.000	0.000 ± 0.000	0.000 ± 0.000	8.029 ± 0.050	7.994 ± 0.051	7.973 ± 0.051	0.000 ± 0.000	3164	1.2	78
ASAS	J060722+0834.0	0.000 ± 0.000	0.000 ± 0.000	0.000 ± 0.000	0.000 ± 0.000	9.401 ± 0.051	9.423 ± 0.050	9.340 ± 0.056	0.000 ± 0.000	3673	1.2	129
OGLE-IV	GD1405.15.132	0.000 ± 0.000	0.000 ± 0.000	0.000 ± 0.000	0.000 ± 0.000	10.852 ± 0.029	10.806 ± 0.029	0.000 ± 0.000	0.000 ± 0.000	6145	0.7	149

Table 1: Classical Cepheids sample.

Subset	$H$ (pc)	$z_0$ (pc)	$N$
$R < 10$ kpc	80.8 +/- 2.8	24.6 +/- 2.8	900
$R < 10$ kpc, Age < 30 Myr	77.9 +8.4/-6.6	16.5 +9.0/-9.7	110
$R < 10$ kpc, 30 < Age < 50 Myr	69.3 +/- 4.9	17.4 +4.8/-4.4	220
$R < 10$ kpc, 50 < Age < 70 Myr	63.3 +4.1/-3.7	22.5 +4.1/-4.5	269
$R < 10$ kpc, 70 < Age < 90 Myr	81.1 +6.1/-5.5	33.8 +7.5/-6.0	185
$R < 10$ kpc, 90 < Age < 110 Myr	91.6 +17.5/-13.9	39.2 +14.7/-14.0	37
$R < 10$ kpc, Age > 110 Myr	177.1 +22.0/-18.5	58.8 +26.4/-24.2	79
$d < 8$ kpc	90.9 +/- 2.8	25.3 +/- 2.8	1111
$d < 10$ kpc	104.0 +/- 3.1	28.6 +/- 2.8	1313

Table 2: Best-fit parameters.  $R$  is the distance from the Galactic Center,  $d$  is the distance from the Sun.